Footprint Catalysis. IX.[1—8] Molecular Footprint Catalytic Cavities Imprinted with Chiral Hydantoins; Enantioselective Hydantoinase Mimics

Tamae MATSUISHI, Toyoshi SHIMADA, and Kensaku MORIHARA*
Department of Chemistry, Faculty of Science, Nara Women's University, Kitauoyanishi-machi, Nara 630
(Received July 22, 1993)

Imprinting using chiral 5-phenyhydantoins ((5*R*)- and (5*S*)-5-pheny-2,4-imidazolinedione) as templates could mark chiral molecular footprint-like cavities on a silica (alumina) gel surface. These cavities displayed evident enantioselective catalyses in reactions of (*R*)- and (*S*)-*N*-carboxyphenylglycine anhydrides, and (*R*)- and (*S*)-5-phenylhydantoins with 2,4-dinitrophenolate, respectively. A proposed mechanism and temperature effects on catalysis suggested that the enantioselectivities depended on the binding step of the catalysis.

We have developed a molecular imprinting method for designing "silica (alumina) gel" catalysts.[1—10] Their active sites are cavities on the silicate surface referred to as "footprints" of template molecules used in the imprinting. They comprise complementary structures to the template molecule and a Lewis acid site at their bottom. These cavities display unprecedented catalytic functions based on their molecular recognition capabilities. According to the structures of the template molecules, they show unique catalytic behavior, i.e., substrate specificities,[1—4] enantioselectivities,[6,9,10] and feedback regulation.[6] Among them, the enantioselective catalyses are significant both theoretically and practically. In a previous study of this series,[10] we found the imprinting with a cyclic derivative of (*R*)-mandelic acid ((−)-(5*R*)-5-phenyl-2,4-oxazolidinedione **5**. Scheme 1) provided chiral footprint cavities. They could catalyze enantioselectively the cleavage of corresponding substrates, (*R*)- and (*S*)-*N*-carboxyphenylglycine anhydrides **2** (Scheme 1). This study intended to use a chiral mandelic acid as a chiral source because of its easy availability. For the matching with *N*-carboxyphenylglycine anhydrides, however, 5-phenylhydantoins ((5*R*)- and (5*S*)-5-phenyl-2,4-imidazolidinedione **1**. Scheme 1) should be better templates than **5**.

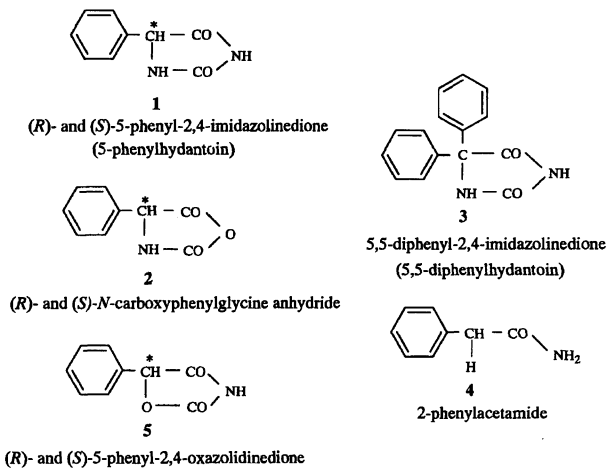

Scheme 1. Templates, substrates, and inhibitors.

This manuscript deals with enantioselective catalyses over footprint catalytic cavities imprinted with the 5-phenylhydantoins. It also describes the enantioselective catalytic cleavages of the (*R*)- and (*S*)-**1** themselves. These unexpected reactions are the first cases where the template molecules themselves serve as substrates in catalytic conditions.

Experimental

Apparatus. IR (KBr) spectra, UV absorption spectra, and ^{1}H NMR spectra were obtained using a Perkin–Elmer 1740 FTIR spectrometer, Shimadzu UV-160 spectrometer, and JOEL GX 270, respectively. pHs were measured using Horiba F-7 pH meter with #6326 electrode.

Materials. All chemicals were of the guaranteed grade of Nacalai Tesque Co., Ltd., if not specified.

Silica Gel: Merck Kieselgel 60, art. no. 7754, particle size 0.06—0.20 mm, mesh 70—230, was used for imprinting. Kieselgel 60 F_{254}, DC-Alufolien, art. 5554, was used for thin-layer chromatography.

Templates: (5*R*)- and (5*S*)-5-phenyl-2,4-imidazolinedione, (*R*)-**1** and (*S*)-**1**, were prepared as described in the literature.[11] (*R*)- or (*S*)-phenylglycine (1.51 g, 10 mmol) and potassium cyanate (0.97 g 1.2 equiv) were suspended in water (10 cm^3), and the mixture was kept at 70 °C with stirring for 30min. The mixture was left to yield crystalline products. (Yields of the crude products: (*R*)-**1**; 84.7%, (*S*)-**1**; 77.8%). The products were recrystallized from ethanol. (*R*)-**1**: Yield; 0.47 g (26.7%), mp 185—186 °C (lit,186 °C). $[\alpha]_D$ −111.6°(*c* 2, ethanol). IR (KBr): 3304, 3213 (amide NH), 1787, 1724 (cyclic amide), 742 and 694 cm^{-1} (CH, phenyl). ^{1}H NMR ($CDCl_3$) δ=4.93 (CH), 7.31 (ArH), 7.61 and 10.27 (NH). (Calcd as $C_9H_8O_2N_2$: C, 61.36; H, 4.55; N, 15.19%. Found: C, 59.83; H, 4.77; N, 15.68%). (*S*)-**1**: Yield; 0.51 g (29.0%), mp 184.5—185.5 °C. $[\alpha]_D$ +111.6°C (*c* 2, ethanol). IR and ^{1}H NMR spectra were the same as those of (*R*)-**1**.

Substrate: (*R*)- and (*S*)-*N*-carboxyphenylglycine anhydrides, (*R*)- and (*S*)-**2**, were prepared from (*R*)- and (*S*)-*N*-benzyloxycarbonylphenylglycine, respectively, as described in the literature.[12] The starting materials were obtained by the usual benzyloxycarbonylation from (*R*)- and (*S*)-phenylglycine, and had the following properties: IR (KBr) 1669

(amide I), 1534 (amide II), 1249 cm^{-1} (amide III). (*R*); mp 124—127 °C, $[\alpha]_D$ −112.0° (*c* 2, ethyl acetate), (*S*); mp 127.5—129 °C, $[\alpha]_D$ +115.5° (*c* 2, ethyl acetate). To a suspension of (*R*)- or (*S*)-phenylglycine (2.85 g, 10 mmol) in benzene (40 cm^3), was added thionyl chloride (1.46 cm^3, 2 equiv) under vigorous stirring. The mixture was kept at 45 °C for 3 h. Then it was concentrated to dryness in vacuo. Addition of petr. benzin gave crystalline product **2**. Then **2** was recrystallized from ethyl acetate-petr. benzin. Yield of (*R*)-**2** was 1.43 g (80.8%), mp 116—118 °C, and that of (*S*)-**2** was 1.43 g (80.8%), mp 116—119 °C. IR (KBr) (R) 3235 (NH), 1846, 1783 (anhydride), 762 and 703 cm^{-1} (CH, phenyl). ^{1}H NMR ($CDCl_3$) δ=5.37 (CH), 6.29 (NH), 7.54 (ArH). (Found: (*R*); C, 61.00; H, 3.95; N, 7.91%). (*R*); $[\alpha]_D$ −125.1°. (*S*); $[\alpha]_D$ +137.2°(*c* 2, ethyl acetate).

Inhibitors: 5,5-Diphenylhydantoin(5,5-dipphenyl-2,4-imidazolinedione **3**) of the guaranteed grade was purchased from Nacalai Tesque Co., Ltd. 2-Phenylacetamide **4** was purchased from Wako Pure Chemical Industries Ltd. They were used without further purification.

Solvent: Acetonitrile, previously dehydrated over calcium chloride, was dried over phosphorus pentaoxide overnight. It was distilled using a Hempel fractionating column, bp 81—82 °C. To the distillate was added calcium hydride, and repeated distillation gave water- and acidic impurity-free acetonitrile.[3)]

Nucleophile: Potassium 2,4-dinitrophenolate, prepared by neutralization of 2,4-dinitrophenol in methanol with concd aqueous potassium hydroxide, was recrystallized from hot water, and dried at 130 °C in vacuo.[3)]

Catalyst Preparation. The preparation procedures were the same with those previously reported in detail.[3,7)] They included successive surface activation, aluminium ion doping, imprinting with templates, drying, and methanol extraction. Kieselgel (120 g) was refluxed with conc hydrochloric acid (500 cm^3) for 3 h to activate the gel surface to generate free silanol groups . The gel was repeatedly washed with deionized water till the washing reached near pH 6.0. Then it was washed with dil aqueous ammonia of pH 7—8 three times, and again washed with water three times. To the washed gel sludge, was added aqueous solution of $AlCl_3 \cdot 6H_2O$ (0.2 mol dm^{-3}, 50 cm^3 to 10 g dry weight of the gel). The pH of the mixture was adjusted to 6.5 with dil aqueous ammonia. The mixture was kept at 80 °C for 3 h. This Al^{3+} ion doping should cause an isomorphical substitution of silicate by aluminate to generate Lewis acid sites on the gel surface. The doped gel was isolated by decantation from precipitated aluminium hydroxide, and washed with dil hydrochloric acid (pH 4.0) till the supernatant became clear. This gel preparation would be referred to as "silica(alumina) gel" in the text, because only it should have superficially silica–alumina structures. Then it was imprinted with a template. To a gel portion (equivalent to 10 g of dry weight) was added an acetone solution of a template (1.5×10^{-3} mol in minimum amount of acetone). The pH of the mixture was adjusted to pH 4.0 with dil hydrochloric acid (pH 1.0) and dil aq ammonia (pH 10—11). The mixture was kept at room temperature for a week with occasional pH adjustment. The gel sludge was isolated from the supernatant and deposited template by decantation, and then washed with dil hydrochloric acid (pH 4.0) 10 times. The gel sludge was collected carefully by filtration so that the gel surface was always kept wet. Then it was dried on Petri dishes at room temperature until it reached a constant weight. It took about 10 days. The dried gel thus obtained was extracted with methanol using a Soxhlet extractor. This continual extraction caused forced removal of template molecules from the silicate surface, which left molecular footprint cavities on the surface. Finally the extracted gel preparation was dried, first in a desiccator at room temperature under atmospheric pressure overnight. Then it was exhaustively dried at 140 °C under reduced pressure (3 mmHg, 1mmHg=133.322 Pa) for 1 h. The fully dried gel samples were immediately used for subsequent kinetic studies. Similar procedures, only omitting a template in acetone, gave the control gel catalysts, which had only Lewis acid sites, lacking complementary structures around them.

Product Analysis. Absorption spectroscopy and isolation on a thin-layer chromatogram were done to confirm the catalyzed reaction products. Equal volumes of an acetonitrile solution of the substrate **1** or **2** (8.33×10^{-3} mol dm^{-3}) and an acetonitrile solution of the nucleophile were mixed. The mixtures showed no change in absorption spectrum in the range of 200—500 nm. To the mixtures was added a silica(alumina) gel catalyst imprinted with (*S*)-**1** (100 mg). To another mixture, was added one drop of $BF_3 \cdot Et_2O$ catalyst as a control experiment. The reaction mixtures were kept at room temperature for 2 h under stirring, and their changes in absorption spectra were recorded at proper intervals. The reaction mixtures were thin-layer chromatographed and developed with benzene. A UV-absorbing spot of a product near the original line was observed on each chromatogram that turned yellow on contact with gaseous ammonia. The ether extracts of the spots were then transferred onto KBr powder for pellets. After ether was evaporated, KBr was pressed into pellets, and they were analyzed by FTIR spectroscopy. Their IR spectra were identical; 1729 (CO–O), 1637 (NH), 1455 (NO_2), 1261, 1098 (CO–O), and 803 cm^{-1} (Ar–H).

Kinetic Measurement. The catalytic activities of the gel were measured by 2,4-dinitrophenolysis of the anhydride substrate **2**, and the hydantoin substrate **1**. The procedures were the same with those previously reported. [3)] Acetonitrile solutions of a substrate(49 cm^3, 0.9—4.5×10^{-3} mol dm^{-3}) was equilibrated with a catalyst (50 mg) at 30 °C or otherwise at a specified temperature for 30 min. The nucleophile solution (1 cm^3, 1.5×10^{-2} mol dm^{-3}) was added to the mixture to start the reaction. The catalyzed reactions were followed by triple-wavelength spectrophotometry. The decreases in optical density of the reaction mixtures at 400, 430, and 500 nm due to 2,4-dinitrophenolate were measured at proper intervals. In inhibition studies, the catalysts were preequilibrated with an acetonitrile solution of an inhibitor for 1 h. Then they were equilibrated with the substrate solutions for additional 10 min. The following procedures were the same as before. Pseudo-first-order rate constants, k_{obsd}, were calculated from the linear part of semi-log plots of optical density vs time that was usually observed over at least the half-life period of the reaction. The k_{obsd}s thus obtained obeyed Michaelis–Menten kinetics with respect to the substrate concentration. Kinetic parameters, K_ms (Michaelis constants), V_{max}s (maximum k_{obsd}s) were calculated from usual double reciprocal plots (Lineweaver–Burk plots), and k_{cat}s were calculated from V_{max} divided by catalytic site

molarity per gram.

Catalytic Site Titration. Catalytic site molarities were measured by the kinetic titration method previously reported.[3] This is based on irreversible poisoning of the catalytic sites with pyridine. The gel catalyst (50 mg) was preequilibrated with specified amounts of pyridine in acetonitrile (5—15 cm^3, 5.0×10^{-5} $mol\,dm^{-3}$) at 30 °C for 1 h under gentle stirring. At this time irreversible poisoning proceeded completely to consume all free pyridine in the mixture. Then the catalytic activities due to surviving catalytic sites were measured as usual, the total volume of reaction mixtures being kept 50 cm^3. The k_{obsd}s obtained were plotted against pyridine molarity. Extrapolation of a linear plot gave an intercept on abscissa. The numerical value of the intercept directly showed the molarity of the catalytic sites per 1 gram of catalyst, since pyridine in 50 cm^3 of the reaction mixtures poisoned a catalyst of 50 mg in these conditions.

Results and Discussion

Template Design. Our previous paper reported that the (*R*)-mandelic acid derivative **5** could mark chiral footprint catalytic cavities.[10] These template molecules (*R*)-**1** and (*S*)-**1** are referred to as isoelectron compounds of **5**. The reasons to choose **1** as templates are the same as those for **5**.[10] That is, i) **1** includes partial structures of –CO–NH–CH(R)–CO– and –CO–NH–CO– in it. Both of them are footprint-forming groups.[1,2,5,9] ii) **1** has large rotatory power due to the phenyl group attached to the chiral center, which will benefit the configuration determination of the reaction products by circular dichroism spectroscopy. iii) **1** is a rigid 5-membered cyclic compound, and the corresponding substrates **2** and **1** are also rigid 5-membered cyclic compounds. The substrates of such rigid structures might have advantages of a small entropy loss on binding onto the catalytic cavities. iv) Acyclic reaction products from the cyclic **2** have distinctly different molecular shapes from **1**. It could prevent rebinding of the products to the cavities, which should cause the product inhibition.[6]

Catalyzed Reactions. Preliminary experiments for product analysis proved that both reactions of the substrates, **2** and **1**, are evidently Lewis acid-dependent; no change in optical density was observed without silica (alumina) gel catalyst or $BF_3{\cdot}Et_2O$. The observed spectrum changes in the catalyzed reactions of **2** and **1** closely resemble those with the benzoic anhydride substrate over footprint cavities.[3] Absorption peaks at 376 and 430 nm diminished rapidly, and new peak of a product emerged at 258 nm. Thin-layer chromatographic analysis found a UV-positive spot of the product near the original line. Since this spot turned yellow on contact with gaseous ammonia, the product should have an active ester (See Scheme 2). The low mobility on chromatogram with benzene suggested the product to be polar. The identical IR spectra of the ether-extracts of the spot from **1** and **2** showed that

< Catalyzed Reaction of *N*-Carboxyphenylglycine Anhydride **2** >

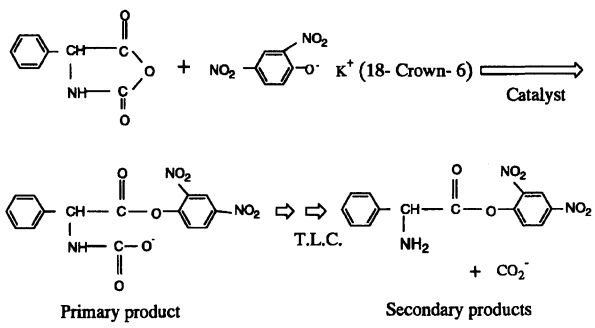

< Catalyzed Reaction of 5-Phenylhydantoin **1** >

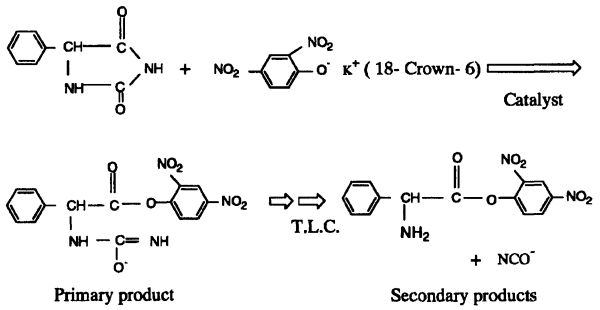

Scheme 2. Catalyzed reactions of **2** and **1**.

the primary products were polar and unstable species. They might leave carboxylate or cyanate, respectively, to yield a common secondary product (2,4-dinitrophenyl ester of phenylglycine). Accordingly the features of the catalyzed reactions should be those as Scheme 2 shows.

Criteria of Footprint Formation. Strong competitive inhibition that occurs by rebinding of the used template have served as a criterion of footprint generation until now. In this catalysis over the cavities imprinted with (*R*)-**1** or (*S*)-**1**, however, this criterion cannot apply, because the templates (*R*)-**1** and (*S*)-**1** were subject to catalyzed reaction with the nucleophile over the cavities imprinted with (*R*)-**1** or (*S*)-**1**. Therefore, enantioselective catalysis observed over chiral footprint cavities itself was used as one of the criteria of footprint generation in this study. This is because a native surface of silica(alumina) gel entirely lacks chiral factors. Another criterion came from competitive inhibition with compounds that are sterically similar to the template but are inert or less reactive to the catalysis. Such inhibitory compounds were **3** and **4**.

Catalytic Behavior to Anhydride Substrates. Figure 1 shows the Lineweaver–Burk plots for the catalyzed reactions of (*R*)- and (*S*)-anhydride substrates ((*R*)-**2** and (*S*)-**2**) over the footprint cavities. The cavities imprinted with (*R*)-**1** template will be referred to as {*R*} from now on. The cavities {*R*} catalyzed the reaction of (*R*)-**2** much more effectively than (*S*)-**2** throughout the entire range of the substrate concentration. Fig-

Table 1. Kinetic Parameters of the Catalyzed Reactions over Footprint Cavities

Catalysts	Substrates	K_m[a] 10^{-4} mol dm^{-3}	V_{max}[b] 10^{-4}s^{-1}	k_{cat}[c] 10^{2}s^{-1}	k_{cat}/K_m[d] 10^{5}mol^{-1}dm^{3}s^{-1}	Enantioselectivities[e]
{*R*}[f]	(*R*)-**2**	1.93	5.64	4.29 (1.20)[g]	22.2	1.34
	(*S*)-**2**	2.14	4.68	3.56 (1.00)	16.6	
{*S*}[h]	(*S*)-**2**	5.26	7.13	4.87 (1.48)[g]	9.25	2.01
	(*R*)-**2**	7.16	4.82	3.29 (1.00)	4.60	
{*RS*}[i]	(*R*)-**2**	5.02	5.45	4.76	9.48	1.0
	(*S*)-**2**	(5.02)[j]	(5.45)	(4.76)	(9.48)	

a) Apparent K_m. b) V_{max} is $k_{obsd\ max}$. c) Divided by molarities of catalytic sites on 50 mg catalysts. d) Substrate specificities of catalytic sites. e) Ratio (*R*)-**1** : (*S*)-**1** of k_{cat}/K_ms. f) 2.63×10^{-5} mol per 1 gram catalyst. g) Relative k_{cat}s; enantioselectivity in the catalytic step. h) 2.93×10^{-5} mol per 1 gram catalyst. i) 2.29×10^{-5} mol per 1 gram catalyst. j) Same as (*R*)-**2**.

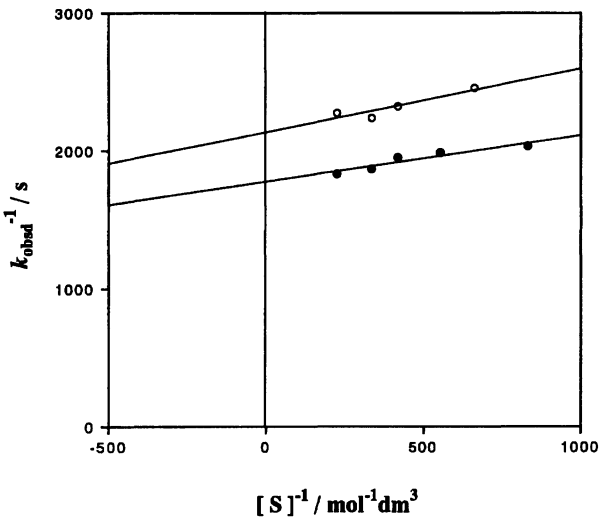

Fig. 1. Lineweaver–Burk plots for the catalyzed reactions of (*R*)- and (*S*)-anhydride substrates over footprint cavities {*R*}. Open circles: (*S*)-**2**. Closed circles: (*R*)-**2**.

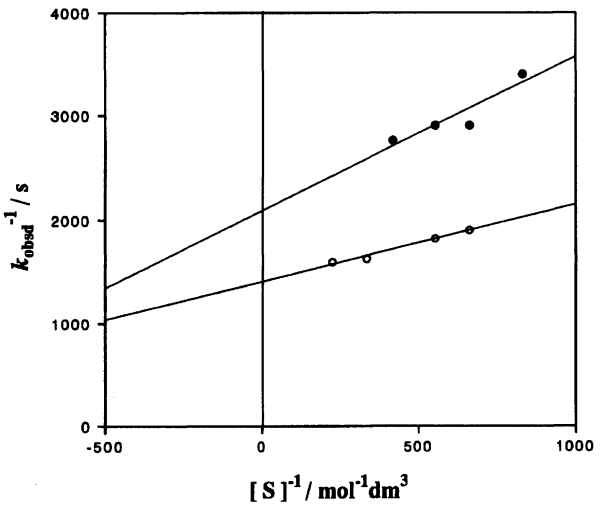

Fig. 2. Lineweaver–Burk plots for the catalyzed reactions of (*R*)- and (*S*)-anhydride substrates over footprint cavities {*S*}. Open circles: (*S*)-**2**. Closed circles: (*R*)-**2**.

ure 2 shows the Lineweaver–Burk plots for the reactions of (*R*)- and (*S*)-**2** over {*S*} (the cavities imprinted with (*S*)-**1**). The cavities {*S*} also displayed an enantioselective catalysis that favor (*S*)-**2**. Figure 3 shows the plots for the reactions of both (*R*)- and (*S*)-**2** over footprint cavities {*RS*} imprinted with racemic **1**. Two plots are almost identical within experimental errors; no enantioselective catalysis was observed. Since {*RS*} should comprise equal amounts of {*R*} and {*S*}, their opposite enantioselective catalyses would cancel each other. Table 1 summarizes the kinetic parameters of the catalyses. These parameters indicate that the enantioselectivity of the catalysis can be ascribed to both the reaction velocity (k_{cat}) and the binding affinity (K_m^{-1}). The opposite enantioselectivities themselves clearly confirmed that (*R*)- and (*S*)-**1** imprinted chiral footprint cavities on a silica(alumina) gel surface. Furthermore, no inversion of enantioselectivities was observed to occur in any substrate concentration. This is in contrast to the results previously reported; the reactions of (Z-L-Ala)$_2$O over {(Z-L-Ala)$_2$NH} showed an inversion of enantioselectivity in low substrate concentration.[6] A cyclic substrate **2** gives acyclic products. It would prevent product inhibition due to rebinding of a reaction product onto the cavities. Obviously the disappearance of the product inhibition suggests that this template design is proper and successful.

Catalytic Behavior to Hydantoin Substrates. The first CO–NH bond fission is evidently a Lewis acid-catalyzed reaction, because this reaction never proceeds without BF_3·Et_2O or silica(alumina) gel catalysts. Figure 4 shows the Lineweaver–Burk plots for the catalyzed reactions of (*R*)-, (*S*)-, and (*RS*)-**1** over the control catalyst. Since their catalytic sites should be native Lewis acid sites without cavity structures, they could not differentiate among the three substrates and had almost identical catalytic activities to them. Figure 4 also displays the catalyzed reactions in the presence of **3** and **4**, respectively. Two compound showed no inhibitory effects at all. These two compounds could be competitive inhibitors, because they are inert or less reactive to the catalysis though they involve partial structures of the template. If cavities hold complementary struc-

Table 2. Kinetic Parameters of the Catalyzed Reactions over Footprint Cavities and Control Catalyst

Catalysts	Substrates	K_m[a] 10^{-4} mol dm^{-3}	V_{max}[b] 10^{-4}s^{-1}	k_{cat}[c] 10^{2}s^{-1}	k_{cat}/K_m[d] 10^{5}mol^{-1} dm^{3} s^{-1}	K_i[e] 10^{4}mol dm^{-3}	Enantioselectivities[f]
{*R*}[g]	(*R*)-**1**	12.80	8.82	5.11 (1.33)[h]	3.99	3.22,[i] 1.87[j]	2.12
	(*S*)-**1**	20.40	7.44	3.84 (1.00)	1.88		
	(*RS*)-**1**	13.04	7.15	4.14 (1.07)	3.18		
{*S*}[k]	(*S*)-**1**	4.79	5.79	3.49 (1.31)[h]	7.28	0.96,[i] 1.09[j]	
	(*R*)-**1**	8.37	4.41	2.66 (1.00)	3.18		2.29
	(*RS*)-**1**	6.37	4.60	2.77 (1.04)	4.35		
Control[l]	(*R*)-**1**	9.12	5.23	4.24	4.65	no inhibition	
	(*S*)-**1**	10.60	5.57	4.51	4.25		
	(*RS*)-**1**	6.56	4.65	3.77	5.75		

a) Apparent K_m. b) V_{max} is $k_{obsd\ max}$. c) Divided by molarities of catalytic sites on 50 mg catalyst. d) Substrate specificities of catalytic sites. e) Competitive inhibition constants. f) Ratio (*R*)-**1**:(*S*)-**1** of k_{cat}/K_m. g) 3.45×10^{-5} mol per 1 gram catalyst. h) Relative k_{cat}s; enantioselectivity in the catalytic step. i) K_i of inhibition by 5,5-diphenylhydantoin **3**. j) K_i of inhibition by 2-phenylacetamide **4**. k) 3.32×10^{-5} mol per 1 gram catalyst. l) 2.47×10^{-5} mol per 1 gram catalyst.

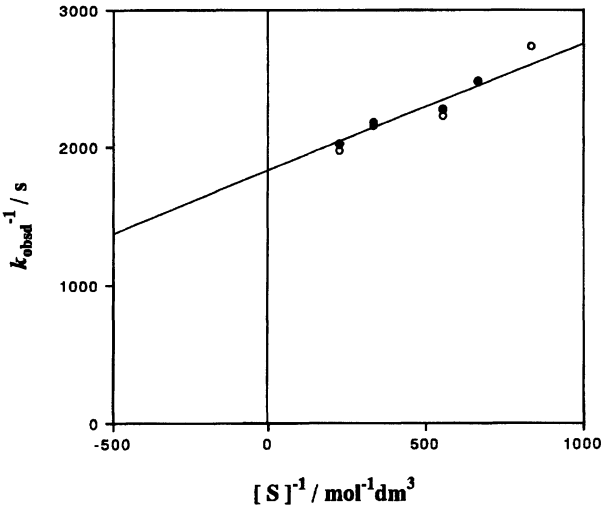

Fig. 3. Lineweaver–Burk plots for the catalyzed reactions of (*R*)- and (*S*)-anhydride substrates over footprint cavities {*RS*}. Open circles: (*S*)-**2**. Closed circles: (*R*)-**2**.

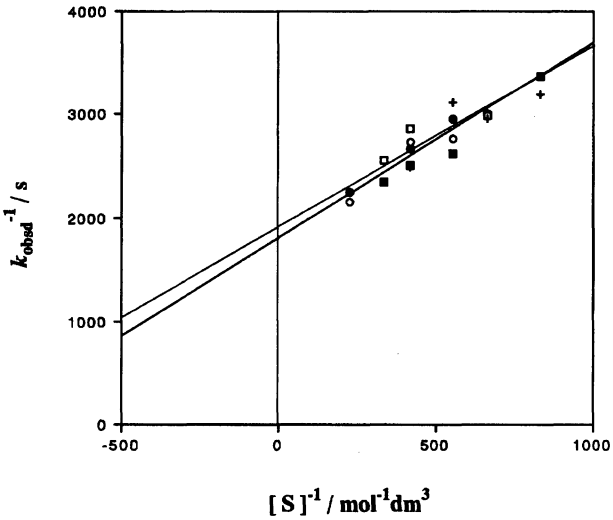

Fig. 4. Lineweaver–Burk plots for the catalyzed reactions of (*R*)-, (*S*)-, and (*RS*)-hydantoin substrates over the control catalyst. Open circles: (*S*)-**1**. Closed circles: (*R*)-**1**. Open square: (*RS*)-**1**. Closed squares: (*R*)-**1** with inhibitor 5,5-diphenylhydantoin, **3** ; [I]= 2.0×10^{-4} mol dm^{-3}. Crosses: With the inhibitor 2-phenylacetamide, **4** ; [I]$=2.0\times10^{-4}$ mol dm^{-3}. Line plottings for open squares, closed squares, and crosses are omitted for simplicity.

tures to **1**, they should have a typical competitive inhibition pattern. Figure 5, the Lineweaver–Burk plots for the reactions of (*R*)-**1** over {*R*} with and without the inhibitors **3** and **4**, evidently has such an inhibition pattern. Figure 6, the similar plots for the reactions of (*S*)-**1** over {*S*} with and without the inhibitors **3** and **4**, also displays such an inhibition pattern. These competitive inhibition patterns observed evidently prove the cavity formation with the use of **1** again. Figure 7 shows the Lineweaver–Burk plots for the reactions of (*R*)-, (*S*)-, and (*RS*)-**1** over {*R*}. The cavities {*R*} showed catalytic activities to these substrates in the order (*R*)>(*RS*)>(*S*); they showed clear stereoselective catalysis. Figure 8 shows similar plots for the reaction of (*R*)-, (*S*)-, and (*RS*)-**1** over {*S*}. The cavities {*S*} showed also evident stereoselective activities here in the reversed order of (*S*)>(*RS*)>(*R*). Table 2 summarizes the kinetic parameters of the catalyses. Cavities {*R*} and {*S*} show opposite enantioselective catalyses for (*R*)-**1** and (*S*)-**1**. The selectivities were the similar to those for (*R*)-**2** and (*S*)-**2** (Table 1); no inversion of the selectivities was observed.

Since enantiomeric templates ((*R*)-**1** and (*S*)-**1**) imprint the cavities, {*R*} and {*S*} should be also enantiomeric in principle. Therefore, they should have finely identical catalytic behavior except opposite and symmetrical enantioselectivities. The observed selectivities, however, did not hold exact symmetricities though they were clearly opposite in direction, as Tables 1 and 2 show. Two reasons are possible. First, par-

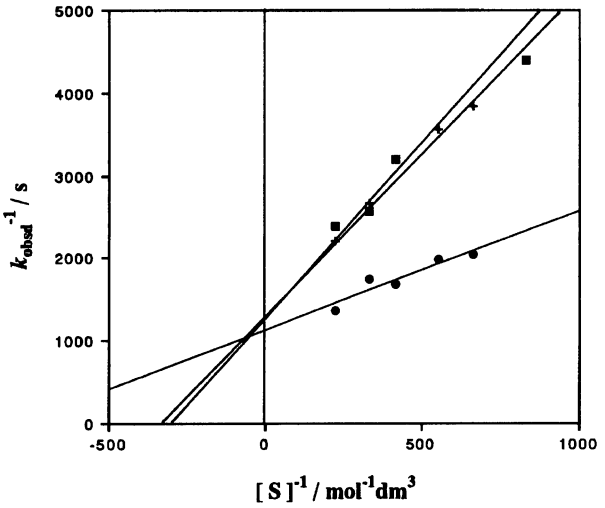

Fig. 5. Competitive inhibition over footprint cavities $\{R\}$. Closed circles: (R)-**1** without an inhibitor. Closed squares: (R)-**1** with the inhibitor **3**; [I]= 2.0×10^{-4} mol dm^{-3}. Crosses: With the inhibitor 4; [I]=2.0×10^{-4} mol dm^{-3}.

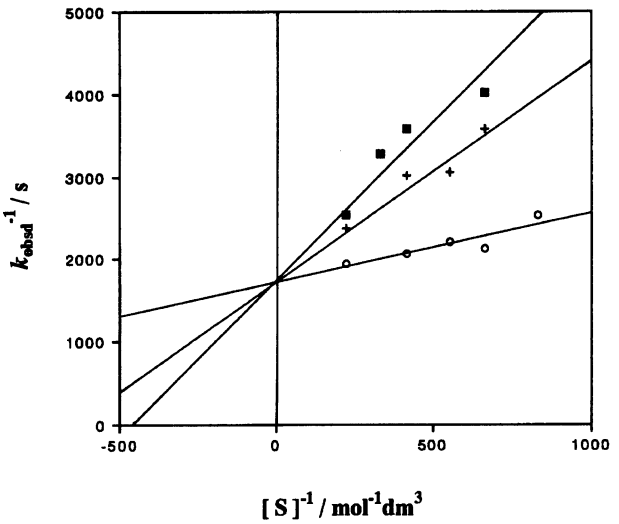

Fig. 6. Competitive inhibition over footprint cavities $\{S\}$. Open circles: (S)-**1** without an inhibitor. Closed squares: (S)-**1** with the inhibitor 3: [I]= 2.0×10^{-4} mol dm^{-3}. Crosses: With the inhibitor 4; [I]=2.0×10^{-4} mol dm^{-3}.

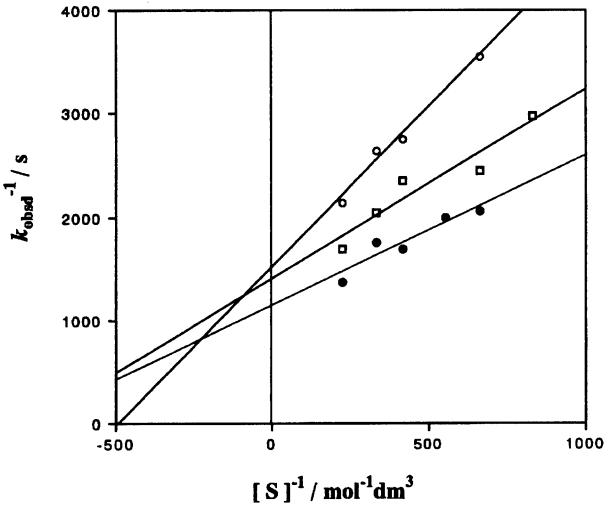

Fig. 7. Lineweaver–Burk plots for the catalyzed reactions of (R)-, (S)-, and (RS)-hydantoin substrates over footprint cavities $\{R\}$. Open circles: (S)-**1**. Closed circles: (R)-**1**. Open squares: (RS)-**1**.

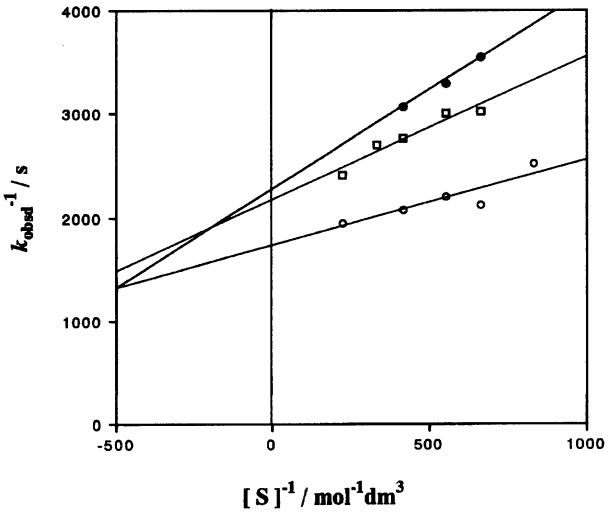

Fig. 8. Lineweaver–Burk plots for the catalyzed reactions of (R)-, (S)-, and (RS)-hydantoin substrates over footprint cavities $\{S\}$. Open circles: (S)-**1**. Closed circles: (R)-**1**. Open squares: (RS)-**1**.

tial recemization of the template molecules might occur during the imprinting process. It would result in unsymmetrical enantioselectivities. Secondly, different chiral recognition capabilities of the cavities might affect the enantioselectivities. Precision of the footprint cavities depends on delicate imprinting conditions, e. g., an imprinting gives precisely imprinted cavities and another give less precisely imprinted cavities. Cavities with different chiral recognition capabilities might afford unsymmetrical enantioselectivities. Secondly, variedly imprinted cavities might affect the enantioselectivities. That is, since the imprinting depends on delicate imprinting conditions, perfectly reproducible cavity formation is not always possible, and sometimes cavities with slightly varied molecular recognition capabilities are formed. Therefore, the imprinting with the enantiomeric templates might form such cavities that are varied in chiral recognition, which might afford unsymmetrical enantioselectivities. The competitive inhibition constants (K_is) with **3** and **4** can measure the molecular recognition capabilities of the footprint cavities. The K_is in Table 2 suggest the second possibility is likely. This is because the first possibility should require the same values of K_is, since two inhibitors can bind equally on both cavities, but the K_i values of the two inhibitors over $\{R\}$ are 3.22×10^{-4} mol dm^{-3}, and

1.87×10^{-4} mol dm^{-3}, and those over $\{S\}$ are 0.96×10^{-4} mol dm^{-3}, and 1.09×10^{-4} mol dm^{-3}, respectively. The different K_is suggest that $\{S\}$ is more precisely imprinted than $\{R\}$. Therefore, symmetrical enantioselectivities should be lost.

It might be hard to understand why the template **1** can serve as a substrate at the same time. Can such a labile compound that is catalyzable ever imprint its own footprint cavities? Answer to this question might lie both on the chemical nature of hydantoins and on the difference in the conditions between imprinting and catalysis. Hydantoin rings favorably cyclize in acidic media and open in alkaline media.[14] The imprinting requires conditions at pH 4.0 (at room temperature), and nucleophilic species are water molecules with poor nucleophilicity. The imprinting conditions must favor cyclization. On the other hand, the catalysis proceeds in anhydrous acetonitrile at 30 °C. As acetonitrile is an aprotic polar solvent, 2,4-dinitrophenolate as nucleophile must exist as "naked" anions. They are more basic and effective nucleophiles than water molecules in aqueous media. Such stronger nucleophilic species might cause the catalytic cleavage of the hydantoin rings.[14] Thus a substrate itself can serve as a template when the substrate molecules are stable enough in imprinting conditions. This finding extends the scope in choice of template compounds.

Mechanism of Enantioselective Catalyses. Figures 1, 2, 3, 4, 5, 6, 7, and 8, and Tables 1 and 2 show that evident stereoselective catalyses proceed over the imprinted cavities with chiral templates. The chiral recognition of these catalysts never comes from the chiral factor of chiral templates. This is because such templates, if remaining in the cavities, should inhibit strongly the catalytic activities. Therefore the stereoselective catalyses must originate chirally imprinted cavities themselves. The structures of footprint cavities must depend on the absorption postures of template molecules on the silicate surface during the imprinting process. Stuart model examination suggests that two absorption postures are possible. The heterocyclic ring of **1** contains both hydrogen-bonding donors and acceptors, i.e., amide and imide protons, and carbonyl oxygen atoms. They should make maximum interactions with Lewis acid sites and the surrounding silicate matrix. Therefore the heterocyclic ring preferentially adsorbs on the surface. Then the phenyl group attached to the ring can take two possible postures; ascending or descending from the heterocyclic ring place. The former would give cavities that can hold only the heterocyclic ring. On the other hand, the latter would form cavities that comprise two subsites in the cavities. One subsite (subsite **a**) holds the heterocyclic ring and another subsite (subsite **b**) holds the descending phenyl group, as a "Lewis acid-base complex" in Scheme 3 shows. The former cavities should show an enantioselective catalysis according to the "lock and key" mechanism. According to Stuart model examination, the former cavities should reject entirely the binding of substrate molecules with different configurations from that of the template. Thus the former should have exclusive enantioselective catalysis in the manner of "all or nothing". This is against the observed results. Chirally imprinted cavities had considerable catalyses for the substrates of the antipode. Further, the former cavities never explain the strong competitive inhibition caused by **3** on both $\{R\}$ and $\{S\}$. Therefore, the cavities of the former type are not likely, but the cavities with two subsites of the latter type should be true ($\{S\}$ in Scheme 3). Scheme 3 displays a plausible enantioselective mechanism over such cavity structures. This is based on a "productive binding and nonproductive binding mechanism". It was proposed for certain enzymic catalysis,[14,15] and we introduced it to explain successfully similar enantioselective catalyses over footprint cavities.[6,9,10] As Scheme 3 shows, the cavity $\{S\}$ includes two subsites, **a** and **b**. It can fit an (*S*)-substrate molecule in the same absorption posture with the template; the phenyl group lies in the subsite **b**. Then the Lewis acid site can activate a carbonyl group of the substrate, and the nucleophile can attack the carbonyl carbon effectively ("productive binding"). On the contrary, the cavity $\{S\}$ holds an (*R*)-substrate molecule in another posture. Also it preferentially holds the heterocyclic ring in subsite **a**. Then $\{S\}$ cavity excludes the phenyl group from the subsite **b**, the substrate molecule keeping the *R*-configuration. The cavities $\{S\}$ should show less affinity for the (*R*)-substrate in this adsorption posture than to the (*S*)-substrate, because such binding of the (*R*)-substrate lacks partial affinity by the subsite **b**. Further, the phenyl group at the outer space of the cavity might shield the carbonyl group of the reaction center. Then it might retard the approach of the nucleophile by steric hindrance ("nonproductive binding"). This mechanism would be commonly applied to **1** as well as **2**. The cavities $\{R\}$ naturally ought to show opposite enantioselectivity, and the observed results supported it.

As Tables 1 and 2 show, $\{R\}$ displays an enantioselectivity in the catalytic step, i.e., relative k_{cat}s of 1.33 ((*R*)-**1**/(*S*)-**1**), and also that of 1.20 ((*R*)-**2**/(*S*)-**2**). Similarly $\{S\}$ has the selectivities of 1.31 ((*R*)-**1**/(*S*)-**1**), and that of 1.48 ((*R*)-**2**/(*S*)-**2**). These magnitude of enantioselectivities (1.20—1.48) seen in k_{cat}s seem distinctly small as compared to other enantioselectivities that have been observed. The catalyzed 2,4-dinitrophenolysis of (Z-D- and L-Ala)$_2$O over footprint cavities {(Z-Ala)$_2$NH} showed the selectivities of 2.82—3.45.[6,16] The methyl groups of (Z-D-Ala)$_2$O on "nonproductive binding" might stand upright, and then they should effectively shield the carbonyl functions of the reaction center. But the phenyl groups of **1** might stand out of upright making 54 °C (a half of 109° 28′) from the heterocyclic plane. Then they should afford less effective shielding of the carbonyl functions. Thus the poorer

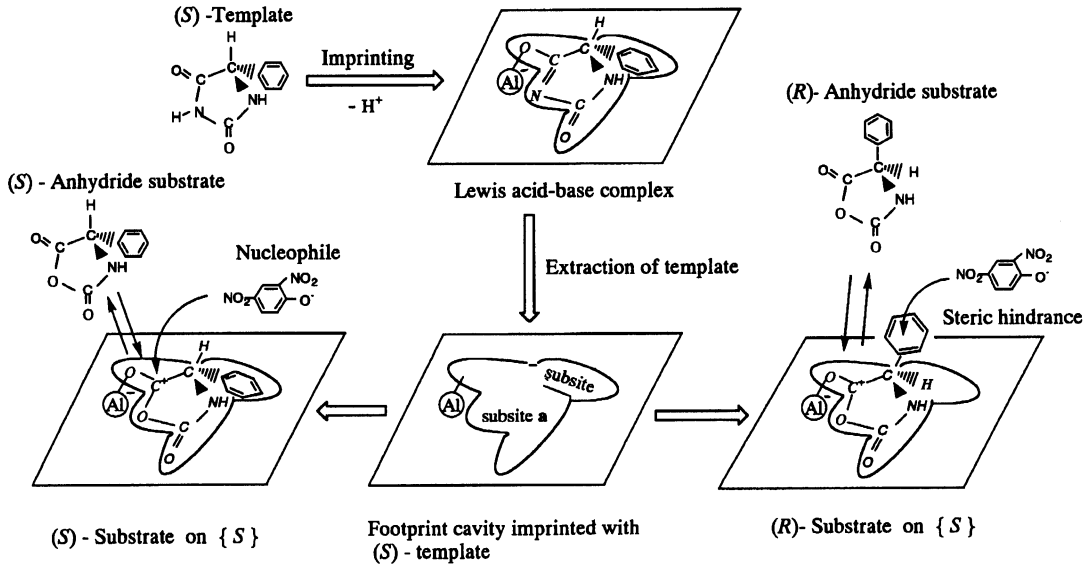

Scheme 3. Enantioselective catalysis over footprint cavities $\{S\}$.

Table 3. Temperature Effect on Catalytic Behavior of Footprint Cavities $\{S\}$[a)]

Substrates	Temperature / °C	K_m[b)] / 10^{-4} mol dm^{-3}	V_{max}[c)] / 10^{-4}s^{-1}	k_{cat}[d)] / 10^{2}s^{-1}	k_{cat}/K_m[e)] / 10^{5}mol^{-1} dm^{3} s^{-1}	Enantioselectivities[f)]
(S)-1	1	1.29	3.10	1.71	13.30	
(R)-1	1	2.15	2.91	1.61	7.50	1.77
(S)-1	9	1.21	3.56	2.40	7.60	
(R)-1	9	5.03	3.72	2.24	4.46	1.70
(S)-1	19	7.25	5.20	2.88	3.97	
(R)-1	19	10.00	4.58	2.54	2.54	1.56
(S)-1	30	13.10	6.71	3.72	2.84	
(R)-1	30	21.60	7.30	4.04	1.87	1.52

a) Catalytic site molarity; 3.61×10^{-5} mol per 1 gram catalyst. b) Apparent K_m. c) V_{max} is $k_{obsd\ max}$. d) Divided by molarities of catalytic sites on 50 mg catalyst. e) Substrate specificities of catalytic sites. f) Ratio (R)-1 : (S)-1 of k_{cat}/K_m.

Table 4. Activation Parameters of the Catalyzed Reaction over Footprint Cavities $\{S\}$[a)]

Substrates	E_a / kJ	$\Delta H_{298}^{\ddagger}$[b)] / kJ	$-\Delta S_{298}^{\ddagger}$[b,c)] / J K^{-1}	$\Delta G_{298}^{\ddagger}$[b)] / kJ	$\Delta G_{total}^{\ddagger}$[d)] / kJ
(S)-1	17.4	15.0	145.9	57.0	38.7
(R)-1	20.3	17.9	136.2	57.1	39.9

a) Catalytic site molarity; 3.61×10^{-5} mol per 1 gram catalyst. b) Activation parameters for the catalytic step. c) Calculated by the values of $\Delta H^{\ddagger}$ and $\Delta G^{\ddagger}$. d) Activation free energy for overall reaction.

steric hindrance would cause poorer selectivities. Alternatively, possible stacking of dinitrophenyl ring of the nucleophile may retard more the steric hindrance to some extent.

Temperature Effects on Enantioselectivities. To investigate further the enantioselective mechanism based on the "productive binding and nonproductive binding" hypothesis, the temperature effects on catalytic behavior were examined. Catalyzed reactions of (R)-**1** and (S)-**1** over $\{S\}$ were done at 1, 9, 19, and 30 °C, respectively. The cavities $\{S\}$ had enantioselectivities that favored (S)-**1** at any temperatures. Table 3 summarizes their kinetic parameters. Temperature change from 30 to 1 °C reduced the k_{cat} by less than a half, but it increased the affinity (nearly equal to K_m^{-1}) of $\{S\}$ to (S)-**1** by more than 10. The temperature sensitive K_m^{-1} term would control the specificities (k_{cat}/K_m) of $\{S\}$ more effectively at low temperatures. Accordingly, such increased specificities of $\{S\}$ could more precisely differentiate small differences between (R)-**1** and (S)-**1** at low temperatures. They should manifest increasing enantioselectivities with de-

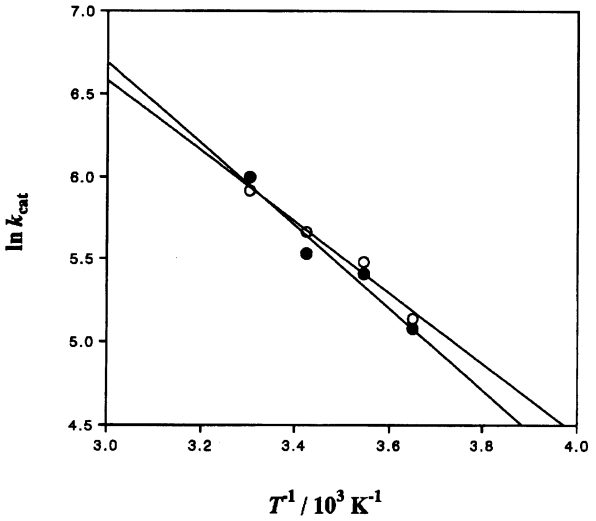

Fig. 9. Arrhenius plots for the catalyzed reactions of (*R*)- and (*S*)-hydantoin substrates over footprint cavities $\{S\}$. Open circles: (*S*)-**2**. Closed circles: (*R*)-**2**.

creasing temperature, as Table 3 shows.

Figure 9 displays the Arrhenius plots, $\ln k_{cat}$ vs. T^{-1}, of these catalyzed reactions. The observed linearities of the plots suggested a common mechanism holds throughout the temperature range. Table 4 shows their activation parameters. The observed activation energy E_a for (*R*)-**1** was 20.3 kJ, and that for (*S*)-**1** was 17.4 kJ. Table 4 shows that the E_as came from the contribution of $\Delta H^{\ddagger}$. Its small difference (2.9 kJ) would correspond to the observed poor enantioselective catalyses.

Conclusion. Chiral 5-phenylhydantoins ((*R*)-**1**, (*S*)-**1**) acted as templates for a molecular imprinting. They successfully marked chiral footprint cavities on a silica(alumina) surface. The cavities, $\{R\}$ and $\{S\}$, showed catalytic activities in both 2,4-dinitrophenolyses of (*R*)- and (*S*)-*N*-carboxyphenylglicine anhydrides, and the cleavages of template molecules themselves. The latter reactions were the first cases where a template served as a substrate. The cavities had evident enantioselectivities; $\{R\}$ prefers the (*R*)-substrates and $\{S\}$ prefers the (*S*)-substrates. A mechanism based on "productive binding and nonproductive binding" hypothesis could explain their enantioselective catalyses. Temperature effects on catalytic reactions also suggested that the enantioselectivities depend on the binding step of the catalysis. These results would extend the scope of the strategy by the our imprinting method.

We would like to thank Dr. Takashi Nakazawa for his helpful advice and discussion.

References

1) Part I: K. Morihara, S. Kurihara, and J. Suzuki, *Bull. Chem. Soc. Jpn.*, **61**, 3991 (1988).
2) Part II: K. Morihara, E. Nishihata, M. Kojima, and S. Miyake, *Bull. Chem. Soc. Jpn.*, **61**, 3999 (1988).
3) Part III: K. Morihara, E. Tanaka, Y. Takeuchi, K. Miyazaki, N. Yamamoto, Y. Sagawa, E. Kawamoto, and T. Shimada, *Bull. Chem. Soc. Jpn.*, **62**, 499 (1989).
4) Part IV: T. Shimada, K. Nakanishi, and K. Morihara, *Bull. Chem. Soc. Jpn.*, **65**, 954 (1992).
5) Part V: T. Shimada, R. Kurazono, and K. Morihara, *Bull. Chem. Soc. Jpn.*, **66**, 836 (1993).
6) Part VI: K. Morihara, S. Kawasaki, M. Kofuji, and T. Shimada, *Bull. Chem. Soc. Jpn.*, **66**, 906 (1993).
7) Part VII: K. Morihara, S. Doi, M. Takiguchi, and T. Shimada, *Bull. Chem. Soc. Jpn.*, **66**, 2977 (1993).
8) Part VIII: K. Morihara, T. Iijima, H. Usui, and T. Shimada, *Bull. Chem. Soc. Jpn.*, **66**, 3047 (1993).
9) K. Morihara, M. Kurokawa, Y. Kamata, and T. Shimada, *J. Chem. Soc., Chem. Commun.*, **1992**, 358.
10) T. Matsuishi, T. Shimada, and K. Morihara, *Chem. Lett.*, **1992**, 1921.
11) T. Suzuki, K. Igarashi, K. Hase, and K. Tuzimura, *Agr. Biol. Chem.*, **37**, 411 (1973).
12) J. P. Greenstein and M. Winitz, "Chemistry of the Amino Acids," John Wiley & Sons, Inc., New York–London (1961), p. 860.
13) E. Ware, *Chem. Rev.*, **46**, 403 (1950).
14) S. A. Bernhard and H. Gutfreund, "Proc. Int. Symp. Enzyme Chem.," Tokyo and Kyoto, 1958, p. 124.
15) C. L. Hamilton, C. Niemann, and G. S. Hammond, *Proc. Natl. Acad. Sci. U.S.A.*, **55**, 664 (1966).
16) K. Morihara and S. Kawasaki, unpublished data.